ISSN: 2790-5306 (Print), 2790-5314 (Online)
IRAQI JOURNAL OF AGRICULTURAL RESEARCH - Ministry of Agriculture
Available online at: www.ijarmoa.gov.iq
VOL. 27 NO. (1) 2023
IJAR
IRAQI JOURNAL OF AGRICULTURAL RESEARCH

ESTIMATION OF WHEAT YIELD ON A FARM IN NAJAF/IRAQ, USING MULTI TEMPORAL SATELLITE IMAGES PAIRS*

M. A. Abdulmajeed [1] **L. A. Al-Ani** [2]

E-mail: mohammed07707926380@gmail.com

ABSTRACT

The present work aims to estimate the yield of wheat crop for a particular wheat farm in Najaf Governorate, southwestern Iraq.

To achieve this objective, seven multispectral bands of the Landsat satellite with a spatial resolution of 30×30 square meters were used for two different time periods. The satellite image for the first time represents the high vegetative growth of the wheat crop, and the satellite image for the second time represents the farm after harvest.

The RGB coloring model was used as an unsupervised method, which classifies the scene according to its three-component RGB color combination. This model was used to determine the number of classes in a scene. Depending on the number of classes determined by the unsupervised method, a supervised classification using a maximum-likelihood technique was used to perform the classification process for the Multi temporal-spectral images. A mask was created to define the selected area (a wheat farm) and through it, the data was read within the boundaries of the area in which the yield will be calculated.

The results show that the rate of wheat production for the study area is equal to 89.27 ton by using spectral bands. It can also be seen that the average percentage error (8.66%) applied with the spectral bands.

Keywords: Wheat production, remote sensing, multi-temporal data, crop yield.

INTRODUCTION

Landsat 9 carries the Operational Land Imager 2 (OLI-2) and Thermal Infrared Sensor 2 (TIRS-2), which were built at NASA's Goddard Space Flight Center in Greenbelt, Maryland [19, 10]. Landsat 9 (in orbit since September 2021), with OLI-2 on board capturing 14-bit radiometric data, this enabled more subtle differences to be detected, particularly in darker regions such as water or dense forests where 16,384 shades could be distinguished at a given wavelength due to the higher radiometric resolution [15].

With the continuous advances in remote sensing technology, satellite sensors can now provide a large number of images with different spectral, spatial and temporal resolutions. In addition, it has become possible to produce dense

* **Part of M.Sc. thesis of the first author.**

[1] **College of Science, Al-Nahrain University, Baghdad, Iraq.**

Received: January 17, 2023
Accepted: March 9, 2023

time-series images with high spectral and spatial resolution for the study of land cover at the Earth's surface and environmental monitoring [15].

Several change detection techniques have been developed, summarized and refined [16, 3, 21, 18, 7]. In addition, D. Lu summarized ten aspects of change detection applications using remote sensing technology [4].

Because of the importance of monitoring change in Earth's surface features, research related to change detection techniques is an active and constantly evolving topic.

The wheat crop is characterized as one of the basic foodstuffs on which a group of individuals who are described as low- or medium-income depend. This fact gave wheat political and military importance that outweighs its economic importance, and economic history is replete with events of countries that fell and collapsed because of grain deals [2].

Wheat and barley production reports are among the important reports for the food security index in Iraq, as wheat is one of the oldest field crops known to be cultivated in the world. Wheat is grown as the main source of food in Iraq in large areas, especially in the northern governorates [1].

Iraq is considered one of the developing countries that meet the requirements of agricultural activity in terms of fertile soil, abundant water and a suitable climate. Wheat in Iraq needs from time to time to be studied and evaluated in order to address problems and inappropriate conditions, and then to develop accurate plans for future visions [2].

The Directorate of Agricultural Statistics in Iraq provides data on various aspects of agricultural activity. The average Donum (1 Donum = 2500 m^2) production of wheat in the irrigated lands was estimated based on the cultivated area (445.5 kg), while the average Dunam production of wheat in arid lands was estimated at 373.8 (kg). Table 1 shows the average yield of wheat (kg/ Donum) for the period (2015-2020) in Iraq [5].

Table 1: Average wheat yield (kg/ Donum) for the period (2015-2020) in Iraq [13]

Details	year	Crop	
		Wheat	Annual percentage change %
Average Yield (Kg/Donum)	2015	637.9	7.6
	2016	825.7	29.4
	2017	705.5	-14.6
	2018	690.5	-2.1
	2019	686.1	-0.6
	2020	727.6	6.0

The field crop surveys carried out by the Directorate are considered one of the largest and most comprehensive seasonal surveys, and they are conducted twice a year (winter and summer), to extract production indicators for the main and secondary field crops.

The directorate provides reports on annual crops, the most important of which are (wheat, barley, cotton, corn and potatoes), in addition to reports of secondary crops and a synthesis report for all crops [5].

This research aimed to calculate wheat production for a specific area. This agricultural area is the wheat farm located in the Najaf governorate in southwest Iraq.

The Study Area:

The wheat farm - which represents the region of interest - is located at 32.08028º N 44.48339º E (path 168 and row 38) in Najaf Ashraf Governorate in the southwestern part of Iraq; it is about 161 km away from the capital, Baghdad. Landsat 8 OLI and Landsat 9 OLI-2 satellite images are used in this study which contains a multispectral band. Two times satellite image was used to show the change in the region which presents the study area. The first-time satellite image was captured in 13th of March 2022, while the second time satellite image was captured in 9th of June 2022.

The study focused on a kind of satellite imagery. They are known as (TM) images and are usually rendered in seven different ranges.

Thematic Mapper (TM) images are an example of such available data, usually provided in seven bands with ground resolution approximately (30 X 30) m^2.

Each ground resolution point has an associated 7-dimensional vector x whose elements are the seven spectral intensities for that particular point.

The elements are generally correlated and each band has a different mean value and each image has 512 x 512 data.

Figure 1a and 1c represents images of TM Bands 1-7 for two times respectively, the x-axis is the column, the z-axis is the row indicator, and the y-axis is the band number or the wavelength of a particular band. Figure 1b and 1d represents a color image of three bands of the studied scene for 1st and 2nd time respectively.

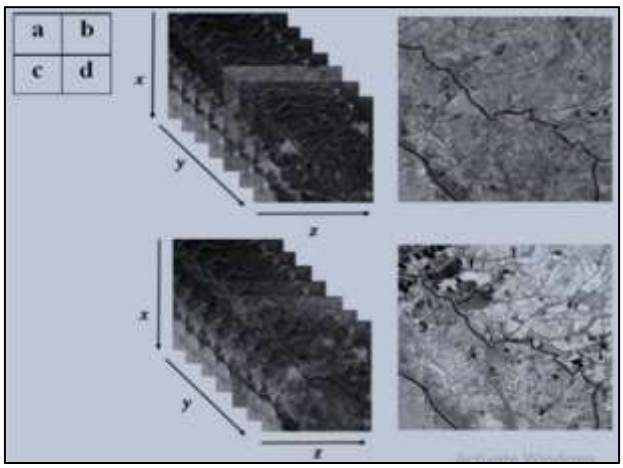

Figure 1: a -multispectral image data (T1), b- Pseudo-color image of (T1), c -multispectral image data (T2), and d- Pseudo color image of (T2)

Multivariate Statistics

Let us consider an image f(x,y), it is represented in the form of one dimensional vector X_i of N^2 elements [14]

$$X_i = \begin{bmatrix} x_{i1} \\ x_{i2} \\ x_{i3} \\ \\ x_{iN^2} \end{bmatrix} \quad (1)$$

Where, X_{ij} denotes the j^{th} component of the vector X_i. The mean of the vector can be determined by the average given by [9]:

$$\mathbf{m_x = E\{x\}} \quad \textbf{(2)}$$

The covariance matrix C_x (is a measure of how well correlated two variables are) of the zero-mean vector x with n components, is given by [20]:

$$\mathbf{C_x = E\{(x - m_x)(x - m_x)^T\}} \quad \textbf{(3)}$$

Where E is the expected value), T: indicates transposition.

Training Site Selection

The first step which is considered as one of the most important concepts of pattern recognition in supervised classification for remote sensing is the correct selection of training sites from which to classify the data. With the approved classification system, supervised classification methods rely on prior knowledge of how many categories are included in the categories in the scene. Training sites were identified to represent each of the required categories in the final outcome.

Unsupervised Classification

The coloring model is adopted as an unsupervised classification. This method allows knowing the number of categories (classes) in Al-Najaf scene for the study area.

The first step in the RGB color transforms requires three bands for input. The RGB color transform uses this input to convert three-band red, green, blue (RGB) images to one of several specific color spaces.

Maximum Likelihood Method

Maximum likelihood classification is the most common supervised classification method used with remote sensing image data [17, 13].

Bayes decision theory is a fundamental statistical approach to the problem of pattern classification [6]. This based on the assumption that training area data sets have a normal distribution (Gaussian in nature), which involves the construction of probability contours [8].

Maximum likelihood rule is a statistical decision criterion for assisting the classification of overlapping signatures; pixels are assigned to the class in which they have the highest probability of being a member [11].

The general multivariate normal density is written as [12]:

$$P(x) = \frac{1}{(2\pi)^{d/2}|\sum|^{1/2}} e^{\left(-\frac{1}{2}Y^T \Sigma^{-1} Y\right)} \quad \textbf{(4)}$$

Where:

$$Y = X - \mu$$

$P(x)$: The probability of pixel vector of (d) elements
μ: The d-component mean vector.
$\sum$: The d-by-d covariance matrix.
T: Superscript indicating transposition.
$\sum^{-1}$: The inverse of the covariance matrix.
$|\sum|$: The determinant of the covariance matrix.

Image Masking:

Image Masking makes it possible to focus on parts of the image that are of interest. Masks can be positioned to highlight certain parts or remove unrelated one's parts of the image. In this project, a mask is built on a specific area of the general landscape to perform calculations on it. This specific area represents the location of the field planted with wheat in the 1st time, and also represents the Harvested Land in the 2nd time.

Since the shape of the region whose production is to be calculated is geometrically irregular, a window has been created that represents the outer boundary of the region, as shown in Figure 2.

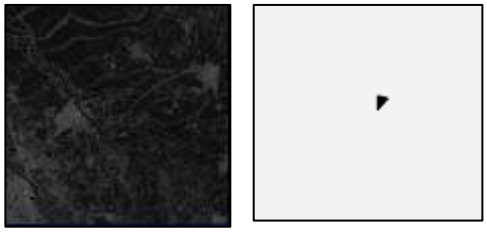

(a) (b)

Figure 2: a) Original satellite band b) a visual representation of a mask created for a particular region in the scene.

To create a mask, a computer program was written to select the region defined by the mask (region of interest). Through this program, data can be read within the boundaries of the region in which the yield will be calculated.

The mask is generated in following steps

1. **Determine the coordinates of the mask borders of the area to be studied.**
2. **Set the value of all pixels outside the mask bounds to 0. Set the value of all pixels inside the mask bounds to 1.**

Figure (3) shows a visual representation of the mask and the process of applying the mask to a specific area created in the scene, as this mask was applied to the image that was classified using a supervised probability classification.

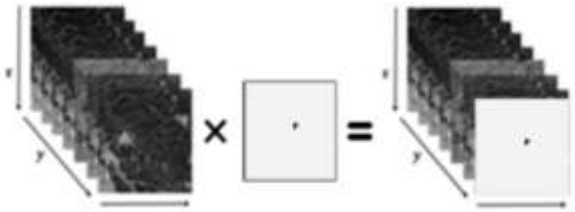

a) 7 channels b) Mask (512 x 512) c) 7 channels

Figure 3: Process of applying mask.

EXPERIMENT RESULTS AND DISCUSSION

The Covariance-variance matrix of the spectral bands for seven bands of the 1st and 2nd time are shown in the table (2) and table (3) respectively.

Table 2: Covariance-variance matrix of the spectral bands (1st time)

Band	1	2	3	4	5	6	7
1	987.2	1126.8	1456.8	2079.9	-211.4	1738.2	2084.6
2		1292.7	1676.2	2404.4	-273.8	2019.7	2414.8
3			2212.7	3182.9	-251.0	2733.7	3219.2
4				4671.3	-595.3	4015.9	4722.7
5					2888.4	200.6	-359.1
6						3971.1	4319.8
7							4972.0

Table 3: Covariance-variance matrix of the spectral bands (2nd time)

Band	1	2	3	4	5	6	7
1	464.1	575.3	849.5	1209.7	995.06	1329.6	1184.5
2		749.07	1135.2	1666.6	1469.6	1939.6	1576.7
3			1784.4	2666.6	2512.7	3190.0	2458.5
4				4105.2	3875.4	5061.3	3777.6
5					5180.2	5253.4	3164.7
6						6968.0	4853.8
7							4077.5

By combination three bands as a Red Green Blue (RGB) the result is a color image, therefore by choosing the SWIR1 band as a red, NIR band as a green and green band as a blue for both image it can get an image showing the vegetation regions in green color as shown in figures 4a and 4b for 1st and 2nd time respectively.

Since the chlorophyll in the vegetation is absorbed the wavelengths of the spectrum in regions of blue and red, and reflected the green and NIR of the spectrum, therefore these bands are chosen to combined as a reason to monitoring the vegetation areas in green color.

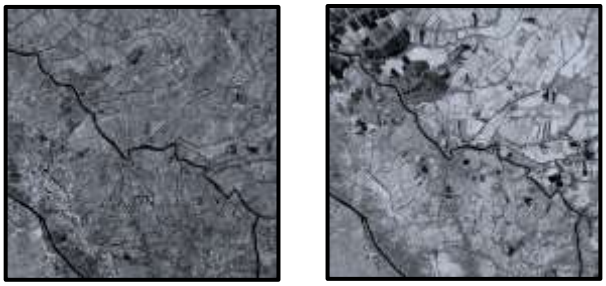

(a) **(b)**

Figure 4: (a) RGB combined image for the 1st time, (b) RGB combined image for the 2nd time.

There are many choices for selecting the three bands between the seven bands, but the traditional method of choosing the three bands comes from choosing the three bands which have the largest variance value.

In Najaf scene and for the first time the three bands which have the largest variance value are bands (7, 4 and 6, sum of variance = 13,614.4). While for the second time the three bands which have the largest variance value are bands (6, 5 and 4 sum of variance = 16,253.4).

Figure 5a and 5b shows two color images for Najaf scene using the RGB model from the bands which have the first three largest variance values for 1st and 2nd time respectively.

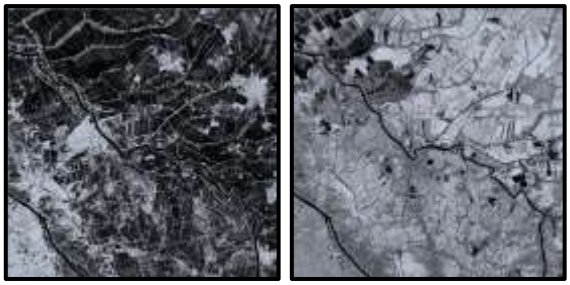

(a) (b)

Figure 5: RGB combined image for the first three largest variance values (a) for the 1st time, (b) for the 2nd time.

Eight classes were adopted, representing distinct categories, and were used to classify this scene with maximum likelihood supervised method.
Six of these classes were validated as different categories identified using the previously mentioned unsupervised method. The remaining two classes are named "Wheat" and "Harvested land" that are the subject of our interest in this study. The list of these eight classes is (classes 1-6, Wheat and Harvested land classes) as be shown in figure 6.

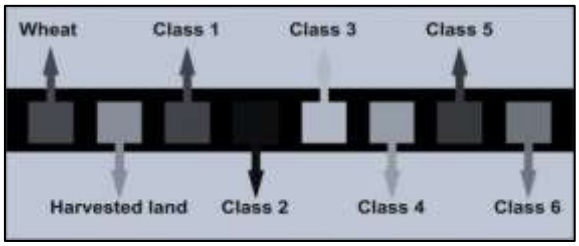

Figure 6: Selected training samples labeled with different colors for the study area (Najaf Scene).

Figure 7 shows the value of reflectance as a function of wavelength for two classes (wheat" and "Harvested Land"). It is evident from Fig. 7 that the infrared wavelengths give the best distinction between the wheat class and the harvested land class.

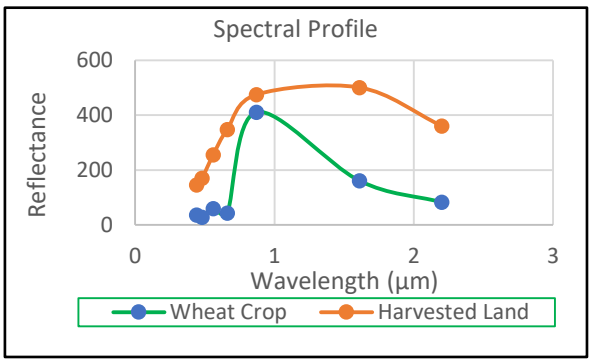

Figure 7: The profile of two classes (Wheat" and "Harvested land").

Maximum likelihood classification was adopted with the original bands for 1st and 2nd time.

Figure 8 shows the results of the supervised classification of maximum likelihood of the seven original bands corresponding to the training areas selected for the first time and for the second time.

Accuracy evaluation is the final step in analyzing remote sensing data that helps us verify the accuracy of our results. Precision relates to the correspondence between the class label and the "real" class.

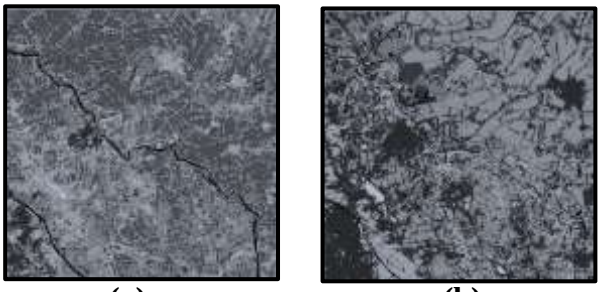

(a) (b)

Figure 8: Supervised classifications of the seven original bands for a) First-time. b) Second time.

The results as presented in Table 4 and 5 showed that the classification accuracy for two original spectral bands 7 and 4 which represent the highest bands in terms of variance was 94.62% and 97.41% for 1st and 2nd time respectively. We can also see that the classification accuracy is reached to a nearly constant level by selecting the three bands with the highest contrast values.

Table 4: Classification accuracy with 1st time

N	Spectral Bands	accuracy %	Kappa %	N	Spectral bands	accuracy %	Kappa%
1	7,4	94.62	93.71	4	7,4,6,5,3	99.58	99.52
2	7,4,6	99.58	99.52	5	7,4,6,5,3,2	99.58	99.52
3	7,4,6,5	99.58	99.52	6	7,4,6,5,3,2,1	99.17	99.03

Table 5: Classification accuracy with 2nd time

N	Spectral Bands	accuracy %	Kappa%	N	Spectral bands	accuracy %	Kappa%
1	6,5	97.41	96.95	4	6,5,4,7,3	100	100
2	6,5,4	100	100	5	6,5,4,7,3,2	100	100
3	6,5,4,7	100	100	6	6,5,4,7,3,2,1	100	100

It was found that the area of the mask is 490,500 square meters (196.2) Donum. The area of the mask-bound region was calculated by multiplying the spatial resolution (30 m x 30 m) by the number of pixels within the mask (545). The mask was applied to the original band images after maximum likelihood supervised classification process.

Table 6 and table 7 show some statistics about Wheat (1st time) and Harvested Land (2nd time) region respectively within the mask applying spectral bands.

Referring to table 6, it is found that the average number of pixels classified as wheat inside the mask is 348 pixels, and by referring to table 7, it is found that the average number of pixels classified as Harvested Land inside the mask is 381 pixels.

Table 6: Statistics about Wheat region within the mask applying spectral bands (Time 1)

N	Spectral Bands	Pixel no. (T1) (wheat)	Area [m^2]	Area [Donum]	Wheat Production [Ton] referring to table 1
1	7,4	300	270000	108.00	76.92
2	7,4,6	288	259200	103.68	73.84
3	7,4,6,5	382	343800	137.52	97.94
4	7,4,6,5,3	375	337500	135.00	96.15
5	7,4,6,5,3,2	365	328500	131.40	93.58
6	7,4,6,5,3,2,1	379	341100	136.44	97.17

Table7: Statistics about Harvested Land region within the mask applying spectral bands(Time 2)

N	Spectral Bands	Pixel no. (T2)	Area [m^2]	Area [Donum]
1	6,5	352	316800	126.72
2	6,5,4	406	365400	146.16
3	6,5,4,7	381	342900	137.16
4	6,5,4,7,3	383	344700	137.88
5	6,5,4,7,3,2	382	343800	137.52
6	6,5,4,7,3,2,1	383	344700	137.88

The mean percentage of wheat yield relative to harvested land within the mask is 91.3% with an average error rate of 8.66%.

REFERENCES

1- Abdel Khalaf, M. and A. A. Rami (2017). “The Impact of Agricultural Policies on the Marketing of Wheat Crop in Wasit Governorate for 2016”, Anbar journal of agricultural sciences, 15 (2), 625-635.

2- Abdulqade, Ammar Mamdooh (2021). “An economic analysis of wheat crop production in Iraq in the context of government support policies and influencing factors for the period (1980-2017)”, Nveo-natural volatiles & essential oils journal| NVEO, p: 2336-2347.

3- Coppin, Pol R. and Marvin E. Bauer (1996). “Digital change detection in forest ecosystems with remote sensing imagery.” Remote sensing reviews 13.3-4: p: 207-234.

4- D. Lu, P. Mausel; E. Brondizio and E. Moran (2003). “Change detection techniques”, int. J. remote sensing, vol. 25, no. 12, 2365–2407.

4- Directorate of Agricultural Statistics / Central Statistical Organization / Iraq, "Production of Wheat and Barley 2020", Report, August (2020).

5- Duda R. O. and P. E. Hart (1973). “Pattern classification and scene analysis”, New York: John Wiley and Sons.

6- Gebeyehu Abebe1; Tsegaye Tadesse and Berhan Gessesse (2022). “Combined Use of Landsat 8 and Sentinel 2A Imagery for Improved Sugarcane Yield Estimation in Wonji-Shoa, Ethiopia”, Journal of the Indian Society of Remote Sensing 50(1), 143–157.

7- Gibson, P. J. and C. H. Power (2000). “Introductory remote sensing: digital image processing and application”, New York.

Gonzalez, R., and R. Woods (2017). “Digital image processing”. New York: John Wiley and Sons.

10- https://www.usgs.gov/landsat-missions/landsat-9."Landsat 9 | U.S. Geological Survey (usgs.gov).

11- Jensen J. R. (2015). "Introductory digital image processing a remote sensing perspective", printice-Hal1, Englewood cliffs, New Jersey.

12- John A. Richards and J. Xiuping (2006). "Remote sensing digital image analysis: An introduction", Springer-Verlag Berlin Heidelberg Printed in Germany.

13- Laith, A. Al Ani1 and Hasan S. Al-Tahir (2020). "Classification performance of TM satellite images", Al-Nahrain journal of science, vol. 23, no.1, p: 62-68.

14- Laith A. Al-Ani (1996)."Classification of digital satellite images", Ph. D. Thesis, Al-Nahrain University.

15- Milad Niroumand-Jadidi, Francesca Bovolo, Mariano Bresciani, Peter Gege and Claudia Giardino, (2022). "Water quality retrieval from Landsat-9 (OLI-2) imagery and comparison to sentinel-2", Remote Sens., vol. 14, pp. 4596.

16- Mouat, D. A.; G. C. Mahin and J. Lancaster (1993). "Remote sensing techniques in the analysis of change detection", Geocarto International, vol. 8, Issue 2, 39–50.

17- Richards J. A. (1984). "Thematic mapping from multi temporal image data using the principal components transform", Remote sensing of environment, vol.16, no. 1, p: 35-46.

18- Serpico, S. B. and L. Bruzzone (1999). "Change detection", Information processing for remote sensing, p: 319-336.

19- Showstack, R. (2022). "Landsat 9 Satellite Continues Half-Century of Earth Observations: Eyes in the sky serve as a valuable tool for stewardship", BioScience 72(3), p: 226-232.

20- Simonds J. f. (1963). "Application of characteristic vector analysis to photographic and optical response data", J, Opt, Soc. Am, vol. 53, p: 968-974.

21- Yuan, D.; C. D. Elvidge and R. S. Lunetta (1998). "Survey of multispectral methods for land cover change analysis", In remote sensing change detection: environmental monitoring methods and applications, edited by R. S. Lunetta and C. D. Elvidge (Chelsea, MI: Ann Arbor Press), p: 21–39.

ISSN: 2790-5306 (Print), 2790-5314 (Online)
مجلة الزراعة العراقية البحثية ـ وزارة الزراعة
متاح على الانترنت: www.ijarmoa.gov.iq
مجلد 27 العدد (1) 2023
IJAR
IRAQI JOURNAL OF AGRICULTURAL RESEARCH

تقدير محصول القمح في مزرعة محافظة النجف/العراق باستخدام أزواج صور الأقمار الصناعية متعددة الأزمنة*

محمد علي عبد المجيد[1] ليث عبد العزيز العاني[1]
E-mail: mohammed07707926380@gmail.com

الملخص

تهدف الدراسة إلى تقدير إنتاجية محصول القمح لمزرعة قمح معينة في محافظة النجف جنوب غرب العراق. لتحقيق هذا الهدف، تم استخدام سبع نطاقات متعددة الأطياف للقمر الصناعي لاندسات بدقة مكانية تبلغ 30×30 متراً مربعاً لمدتين زمنيتين مختلفتين. تمثل صورة القمر الصناعي للزمن الأول النمو الخضري المرتفع لمحصول القمح، وتمثل صورة القمر الصناعي للزمن الثاني المزرعة بعد الحصاد.

تم استخدام أنموذج التلوين (أحمر، أخضر، أزرق) كطريقة للتصنيف غير الموجه، التي تصنف المشهد وفقاً لأنموذج التلوين (أحمر، أخضر، أزرق) المكون من ثلاث مركبات، أذ استخدم هذا الأنموذج لتحديد عدد الفئات في المشهد. اعتماداً على عدد الفئات التي تم تحديدها من طريقة التصنيف غير الموجه، تم استخدام التصنيف الموجه بتقنية الاحتمالية القصوى للأداء لتصنيف الصور متعددة الأطياف/الأزمنة. تم بناء قناع لتحديد المنطقة ذات الاهتمام (مزرعة القمح) ومن خلاله تمت قراءة البيانات داخل حدود المنطقة التي سيتم حساب عائد المحصول فيها.

بينت النتائج أن معدل إنتاج القمح لمنطقة الدراسة ذات الاهتمام يقدر بـ 89.27 طناً باستخدام النطاقات الطيفية. كما اظهرت الدراسة أن متوسط النسبة المئوية للخطأ (8.66٪) عند تطبيقها مع النطاقات الطيفية.

الكلمات الدالة: انتاج القمح، الاستشعار عن بعد، البيانات متعددة الأوقات، إنتاجية المحاصيل

*جزء من رسالة ماجستير للباحث الأول.

[1]كلية العلوم، جامعة النهرين، بغداد، العراق.

تاريخ تسلم البحث:17/كانون الثاني/2023
تاريخ قبول البحث: 9/ اذار/2023